Hindawi
International Journal of Photoenergy
Volume 2023, Article ID 3312619, 9 pages
https://doi.org/10.1155/2023/3312619

Research Article

Monocrystalline Silicon PERC Solar Cell with Rear-Side AlO_x Film Formed by Furnace Oxidation

Ching-Hui Hsu, Da-Yao Lao, and Likarn Wang

Institute of Photonics Technologies, National Tsing Hua University, Hsinchu, Taiwan 300

Correspondence should be addressed to Likarn Wang; lkwang@ee.nthu.edu.tw

Received 19 October 2022; Revised 13 January 2023; Accepted 28 June 2023; Published 17 July 2023

Academic Editor: Regina De Fátima Peralta Muniz Moreira

In this study, AlO_x passivation layers on the rear sides of silicon PERC solar cells are formed by thermally oxidizing 3 nm-thick aluminum films deposited in advance by an e-gun evaporator. The oxidation process is conducted in a furnace full of oxygen at 400°C for a duration of 10 minutes, followed by annealing for a duration of 3 minutes at 700°C, and then the stacking of SiN_x films on the back surfaces. After that, a second annealing process is done at 400°C for a duration of 10 minutes to repair the defects resulting from the bombardment of ions on the passivation layer. With the thermal oxidation method applied, we confirmed the existence of an AlO_x passivation layer with a negative charge density of $-3.21 \times 10^{12}\,cm^{-2}$ for an annealed sample, in contrast to $-6.17 \times 10^{11}\,cm^{-2}$ for an unannealed sample.

1. Introduction

To promote the conversion efficiency of solar cells, PERC (passivated emitter and rear cell) solar cells have attracted the extensive attention of many researchers and manufacturers. To fabricate a p-type PERC, a passivation layer, usually an AlO_x layer, is deposited on the rear side of a silicon solar cell to provide negative charges, giving rise to field-effect passivation. Nowadays, AlO_x layers are deposited by ALD or PECVD facilities in fabricating PERC solar cells with conversion efficiencies of around 20~21% [1–6]. Specifically, Kotipalli et al. reported charge densities of $-5.3 \times 10^{12}\,cm^{-2}$ and $-2.3 \times 10^{12}\,cm^{-2}$ by using plasma-enhanced ALD and thermal ALD equipment, respectively [2], while Hsu et al. used a two-step post annealing process for ALD aluminum oxide films and achieved a charge density of $-2.4 \times 10^{12}\,cm^{-2}$ [3]. In contrast to ALD, PECVD equipment can provide a relatively high deposition rate and has been frequently used by industry [4]. The negative charge density of $-4.2 \times 10^{12}\,cm^{-2}$ was reported for an annealed AlO_x/SiN_x stack deposited by using PECVD [5]. These vacuum facilities, however, are costly and sometimes would deter cell manufacturers from starting a transition into the PERC industry.

Some cost-effective methods for coating AlO_x thin films have been developed, like sputtering, the sol-gel method, AlO_x printing, and oxidation [7–10]. Li and Cuevas deposited an AlO_x passivation layer using an rf magnetron sputtering method with an aluminum target sputtered in an oxygen ambient, obtaining a negative charge density of about $-3 \times 10^{12}\,cm^{-2}$ [7]. Later, García-Valenzuela et al. reported an improved passivation result based on magnetron sputtering with an Al_2O_3 ceramic target used [8]. An excellent surface passivation layer of AlO_x with a negative charge density of $-4.9 \times 10^{12}\,cm^{-2}$ was synthesized with a sol-gel method [9]. Lin et al. used a printable AlO_x paste to form a passivation layer on the back side of a solar cell and obtained a conversion efficiency of 20% [10].

AlO_x passivation layers can be also formed by oxidizing aluminum films deposited on the back side of solar cells. In the study of Liu et al. [11], they used ozone gas to oxidize an aluminum thin film into an AlO_x layer on the back side of a p-type solar cell, obtaining a negative surface charge density of $-2.3 \times 10^{12}\,cm^{-2}$. Then, by introducing second-time annealing for the AlO_x layer, which was performed after the deposition of a PECVD SiN_x capping layer, it was found that such an ozonation method brought about an improvement in both

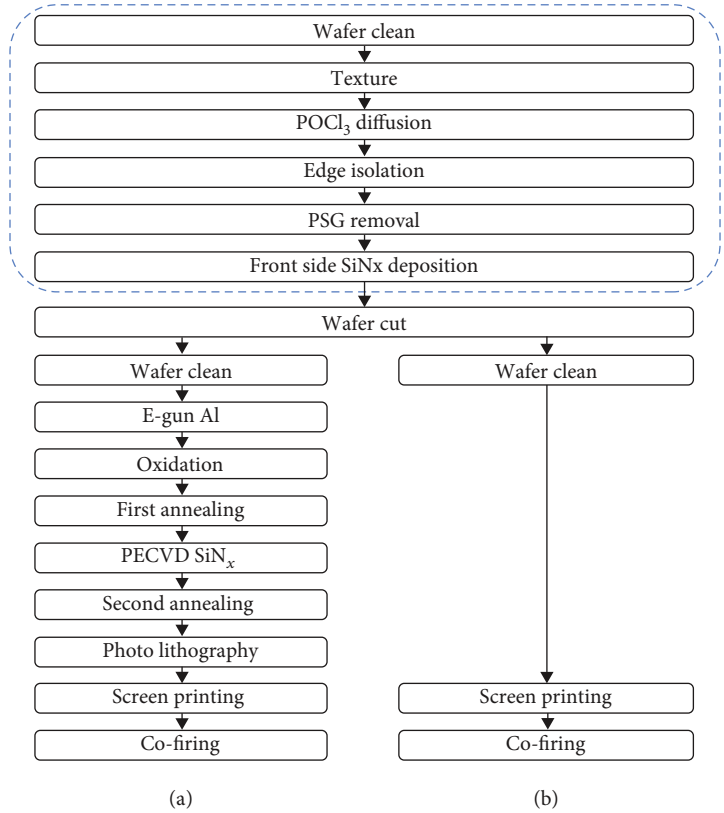

Figure 1: Process flows for fabricating the PERC (a) and control cells (b), the latter of which are cells with an all-over back surface field. The part enclosed by the dash line represents standard commercial processes.

the passivation effect and the solar cell efficiency. In a subsequent study, we further found that the use of thermal oxidation could result in a better passivation effect and hence a further improvement in solar cell efficiency [12]. In this paper, we present the experimental results obtained by using the thermal oxidation method and make a comparison between these two kinds of oxidation methods.

The paper is organized as follows. In Section 2, the process of cell fabrication is introduced, followed by a number of measurements, including minority carrier lifetime measurement to find the optimal processing conditions, TEM/EDS/XPS for compositional analysis of AlO_x/SiO_x layers, and CV measurement to determine the negative charge density. Performances of solar cells are evaluated through the IV test and IQE measurement in Section 3. There, a brief comparison between the ozonation method and the thermal oxidation method is also made. Then, Section 4 concludes this paper.

2. Experiments

2.1. Process Flow of Solar Cell Fabrication. In this study, we used pseudosquare (100)-oriented 200 μm-thick diamond-wire-sawn single-crystalline p-type silicon substrates to fabricate solar cells, following the process flow of fabrication shown in Figure 1, where two splits of sequences appear for the PERC solar cells and the Al-BSF cells, respectively, after the standard commercial manufacturing process up to "front side SiN_x deposition" is finished. Commercial $156 \times 156\,mm^2$ wafers were SC1 cleaned first and then were textured to form pyramids on both sides of the wafers, followed by $POCl_3$ diffusion to form an n layer on each front side. Afterwards, an edge isolation process with a wet chemical etch was conducted to remove the phosphorus layers on the rear sides and edges of the wafers. Then, after phosphosilicate glass (PSG) was removed, antireflection coating (ARC) layers of silicon nitride (SiN_x) were deposited on the front sides of these wafers by plasma-enhanced chemical vapor deposition (PECVD) equipment. These SiN_x-coated wafers are referred to as blue wafers here below.

Then, the blue wafers were cut into smaller samples with dimensions of $5.2 \times 5.2\,cm^2$, followed by a cleaning process with acetone and the SC2 mixture. We put these smaller wafers into the fabrication process of PERC by starting the formation of AlO_x layers on the back sides of the cut samples. A number of lifetime and CV measurements were carried out in order to optimize cell performance. To form AlO_x layers, we deposited 2 film set to be 3 nm, although the genuine thickness could be larger in the deposition of such a thin film [11]. Then, the as-deposited samples were put into a furnace which was full of oxygen for the purpose of oxidation. After the aluminum films were oxidized into AlO_x layers, the wafers were annealed in a sintering furnace to produce negative charges at the AlO_x/Si interfaces. In the end, the samples were measured by the quasisteady state photoconductance method (with WCT-120 equipment) to

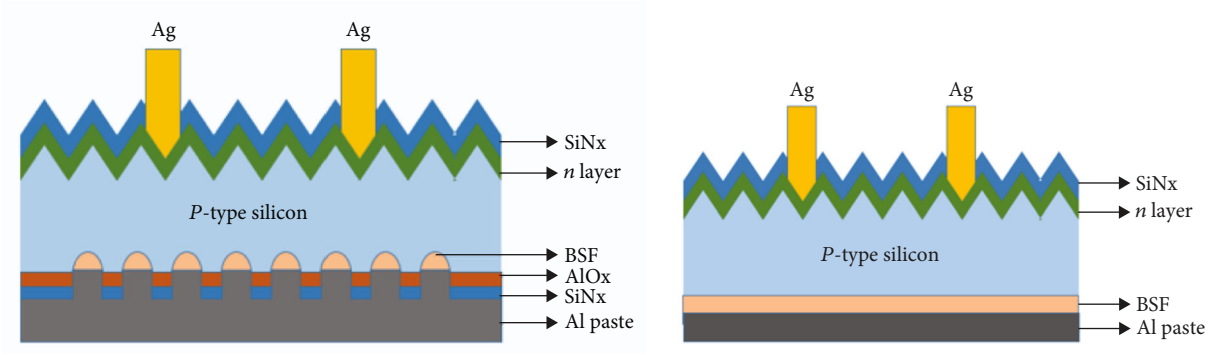

Figure 2: Layer structures of PERC (a) and the Al-BSF cell (b).

find their minority carrier lifetimes. It should be noted that the lifetime measurement in this study was conducted at the minority carrier density of $1.0 \times 10^{15}\,\text{cm}^{-3}$. The annealing process is required for forming a tetrahedral structure at the AlO_x region right next to the SiO_x layer, leaving aluminum vacancies at the SiO_x/AlO_x interface [11, 13]. It is noted that the theoretical thickness of AlO_x was 1.7 times larger than that of metallic aluminum if $x = 1.5$ because of the joining of oxygen atoms.

After the passivation layer was formed, we stacked a 100 nm-thick SiN_x film on the rear surface to protect the passivation layer. And then, we put it into a sintering furnace to do the second annealing process. Such annealing was found necessary for recovering the lifetime back to the level obtained after the wafer was first annealed. A photolithographic process was subsequently employed to form a pattern of line-shaped openings on the rear side. Then, aluminum paste and silver paste were screen printed on the back and front sides of the wafers, respectively, followed by a cofiring process through a conveyor belt furnace to form a local back surface field pattern on the back side and a grid electric contact pattern on the front side. Then, the cells were cut into pieces with dimensions of $2 \times 2\,\text{cm}^2$.

Figure 1 shows the process flows for the fabrication of the PERC and control cells, the latter of which are cells with aluminum paste screen-printed on the rear side without a passivation layer (denoted by Al-BSF cells). Figure 2 shows the layer structures of PERC and the control cell.

2.2. Lifetime Measurement. We oxidized and annealed a number of as-deposited samples to find the optimal time duration and temperature of thermal oxidation. We proceed as follows. In step 1, the minority carrier lifetimes of the test wafers were measured before the AlO_x layers were formed. In step 2, we proceeded with the oxidation for 5 and 10 minutes, respectively, at 300, 400, and 500°C, and then performed annealing processes all at 700°C for 3 minutes in step 3. Afterwards, the lifetimes of these as-annealed wafers (i.e., those with AlO_x layers formed on the back sides) were measured again. Magnification of lifetime, a ratio of the two lifetime values, for each sample was then found as an index in relation to the performance promotion resulting from the passivation effect of the AlO_x layer. Figures 3(a) and 3(b) show the magnification of lifetime for the wafers with back-side AlO_x layers formed at various oxidation temperatures for the cases of 5-minute and 10-minute oxidation durations, respectively. Two samples were tested in each case of oxidation temperature for either a 5-minute or 10-minute oxidation duration. It can be seen from this figure that a maximum magnification of a lifetime of >8.0 was achieved for an as-annealed wafer that was oxidized at 400°C for 10 minutes and subsequently annealed at 700°C for 3 minutes. Note that the maximum value of lifetime read was 42.4 μs for this optimal case. We have also changed the oxidation duration to 20 minutes while keeping the oxidation temperature at 400°C and the same annealing condition. However, the magnification of lifetime could only reach <7.4 maximum, which corresponded to <40 μs. Thus, we chose the oxidation temperature and oxidation duration of 400°C and 10 minutes for this study. Note that the lifetimes measured before the AlO_x layers that were formed were all in the range of 5.2 to 5.6 μs.

Then to find the optimal condition for the first annealing, we tried four annealing temperatures, i.e., 500°C, 600°C, 700°C, and 800°C. Figure 4 shows the magnification of lifetime versus time duration of the first annealing for various annealing temperatures. From the figure, we found that a maximum magnification of 8.9 could be reached by the first annealing at 700°C with a time duration of 3 minutes. Note that such a magnification corresponded to the case of a lifetime of 45.7 μs. At other annealing temperatures, the magnification of lifetime would be lower, indicating that lifetime improvements in these cases were not big enough owing to nonoptimal annealing. Note that the annealing is to rearrange the atomic structure of AlO_x near the Si/AlO_x interface such that AlO_x near the SiO_x has a tetrahedral geometry, leaving insufficient aluminum atoms and producing negative charges. We believe that an insufficient thermal budget due to a lower annealing temperature (e.g., 500°C or 600°C) and/or shorter time duration could cause incomplete generation of AlO_4^- geometry [5]. However, as we can see from the figure, annealing at 800°C with a duration of 3 minutes or at 700°C with a longer duration providing an excessive thermal budget would not produce sufficient negative charges either. Through a series of measurements, we then found the best conditions for thermal oxidation and

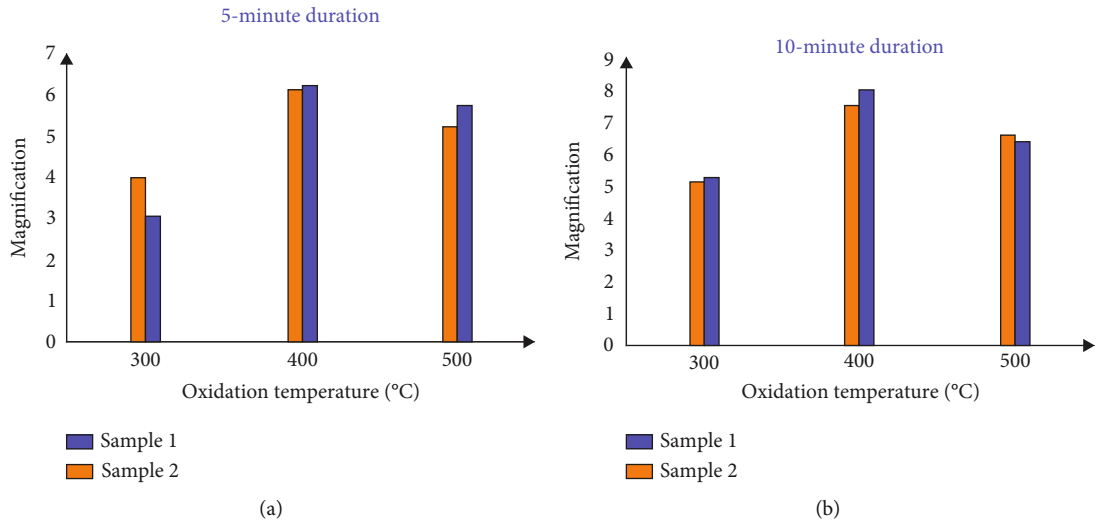

Figure 3: lifetimes measured for the wafers with back-side AlO_x layers formed at various oxidation temperatures for (a) 5-minute and (b) 10-minute oxidation durations, respectively.

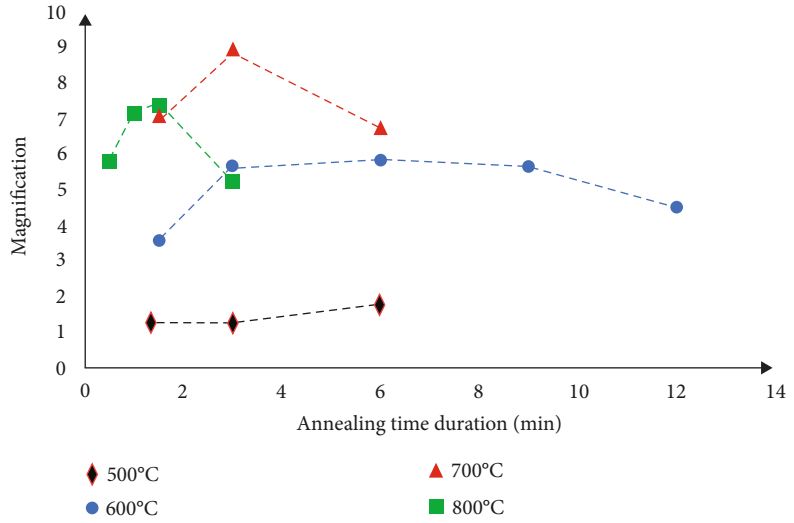

Figure 4: Magnification of lifetime versus time duration of first annealing at 500°C, 600°C, 700°C, and 800°C.

subsequent annealing that led to the longest lifetime. The best condition so far was a 10-minute-long oxidation at 400°C and a subsequent annealing lasting for 3 minutes at 700°C. However, a reduction of 50%~70% in lifetime was observed after the back-side SiN_x was deposited. We measured the lifetimes of 6 as-annealed wafers (see the column of lifetime after first annealing in Table 1). A significant reduction in lifetime could be seen from the second left column after a back-side SiN_x layer was deposited by PECVD, which caused damage to the thin Al_2O_3 layer. Such a problem could be overcome by applying a second annealing. To find the optimal annealing to recover the lifetime back to the original, we divided the 6 wafers into three groups, with each group containing 2 wafers, which were then annealed at 400°C, 500°C, or 600°C, respectively. At each annealing temperature, the 2 wafers were annealed for 10 and 20 minutes, respectively. The resultant lifetime after the second annealing is shown in Table 1 (see the second right column). The recovery percentage was close to unity as the wafer was annealed at 400°C for 10- and 20-minute durations; however, it became 68% to 84% for higher temperature annealing. It is worth noting that the recovery percentage became 55% for wafers annealed at 700°C with a shorter time duration, such as 30 sec or 60 sec. Thus, the best temperature and time duration for the second annealing are 400°C and 10 minutes, respectively. Although high-temperature annealing might release hydrogen bonds to passivate the dangling bonds at the rear surface, reducing interface trap density (D_{it}), the negative charge density would decrease because of positive charges from the hydrogen bonds [14]. Therefore, there exists a proper annealing temperature and time duration for optimizing lifetime. It was reported by [15] that annealing at 450°C led to a minimum D_{it}. Such an annealing temperature is in good agreement with what was found here for optimization.

Table 1: Lifetimes measured after first annealing at 400°C with a time duration of 10 minutes, back-side SiN_x deposition, and after second annealing at various temperatures with a time duration of 10 or 20 minutes. The recovery percentage is defined as the ratio of the lifetime after the second annealing to that after the first annealing.

Lifetime (μs) after first annealing	Lifetime (μs) after back-side SiN_x deposition	Temperature (°C) of second annealing	Time duration (min) of second annealing	Lifetime (μs) after second annealing	Recovery percentage (%)
43.02	18.72	400	10	42.48	99
46.54	18.69		20	45.36	97
43.15	20.88	500	10	36.3	84
45.41	14.77		20	30.93	68
40.39	12.46	600	10	29.72	74
35.81	17.01		20	26.46	74

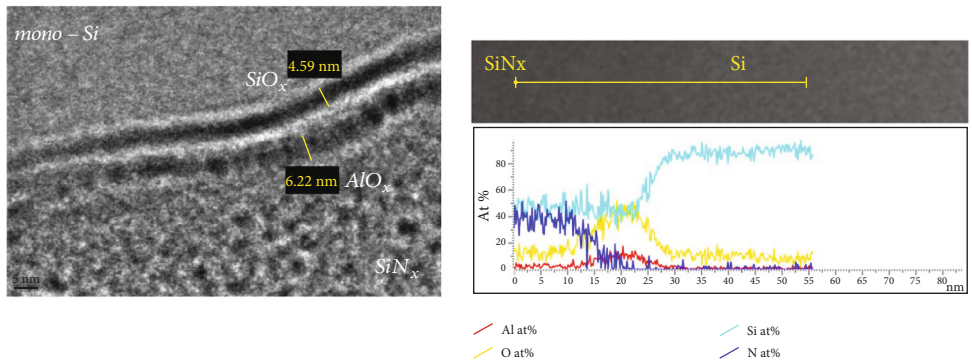

(a) (b)

Figure 5: (a) TEM image taken for a wafer to show layer structure after annealing. (b) Corresponding graph of the elemental composition obtained by EDS measurement.

2.3. Compositional Analysis of AlO_x Layer. Figure 5(a) shows the TEM image of the layer structure after the wafer was oxidized and annealed under the aforementioned optimal condition. A 4.59 nm-thick SiO_x layer was grown beside the 6.22 nm-thick AiO_x layer, which was larger than the thickness of the metallic aluminum with a reason explained previously. Shown in Figure 5(b) is a graph of elemental composition obtained by energy-dispersive X-ray spectroscopy (EDS) measurement. In the EDS graph, the SiN_x capping layer resides in the region of 0 to 15 nm, while the region of 15 to 26 nm contains AlO_x and SiO_x. Notably, the thickness of 11 nm for the oxide layer matches that revealed by the TEM measurement shown in Figure 5(a). However, the boundary between different layers was not sharply clear, and a large number of silicon atoms together with a small number of nitrogen atoms were found throughout the oxide region. The reason for this observation might result from the use of an ion beam to cut the wafer, leaving the two elements transferred to the AlO_x/SiO_x layers.

The composition analysis was also performed by using XPS (X-ray photoelectron spectroscopy) measurement. Figure 6 shows the profiles of atomic composition before annealing (Figure 6(a)) and after annealing (Figure 6(b)). It can be seen that AlO_x was formed with x equal to 1.25 near the surface and always smaller than 1.5 deep inside before annealing. This indicates that there was no tetrahedral structure formed from the surface to the AlO_x/Si interface before annealing. However, after the wafer was annealed, the atomic ratio of oxygen to aluminum became 1.5, indicating the presence of Al_2O_3 near the surface. Then, oxygen was maintained at ~60%, while aluminum atoms started decreasing in number deep inside as the etch time increased from 0 to 40 sec, indicating the presence of AlO_x^-, which justifies the formation of negative charges [5].

2.4. Determination of Negative Charge Density. Figure 7(a) shows the CV testing results for an annealed and an unannealed sample, respectively. Here, the unannealed sample refers to the wafer with AlO_x and SiO_x formed by the aforementioned thermal oxidation method at the optimal condition (i.e., at 400°C and a duration of 10 minutes) without subsequent annealing performed, while the annealed sample refers to that with subsequent annealing performed at 700°C for a duration of 3 minutes. After finding a flat band voltage V_{FB} from the CV relation for each annealing case, we then determined the negative charge density from the following equation as $-3.21 \times 10^{12}\,\mathrm{cm}^{-2}$ for the annealed sample and $-6.17 \times 10^{11}\,\mathrm{cm}^{-2}$ for the unannealed sample.

$$Q_F = \frac{(\varphi_{ms} - V_{FB})\mathrm{Cox}}{qA}. \quad (1)$$

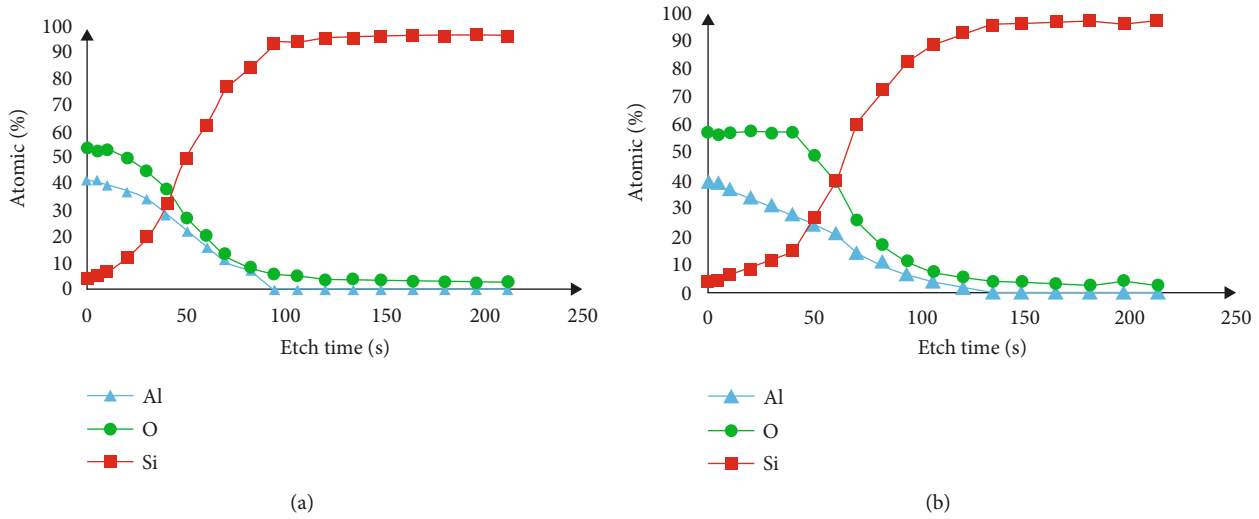

Figure 6: Profiles of atomic composition before annealing (a) and after annealing (b).

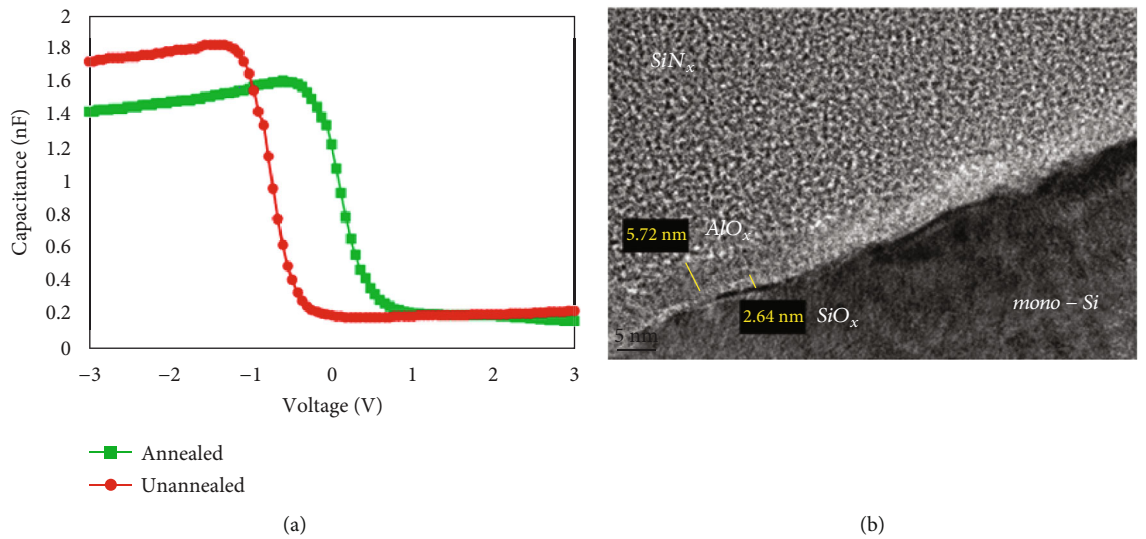

Figure 7: (a) CV relation obtained for an annealed sample (squares) and an unannealed sample (circles). (b) TEM image taken for a wafer to show layer structure before annealing.

In Equation (1), φ_{ms} is the difference in work function between aluminum and the silicon wafer, Cox is the capacitance of the oxide layer, q is the electron charge, and A is the area of the capacitor.

The CV curve of the annealed sample is situated to the right of that of the unannealed sample, with the reason explained in the following. Since the unannealed sample has a thinner oxide layer (see Figure 7(b) in contrast to Figure 5(a)) and accordingly a higher Cox value than the annealed, the flat band voltage would increase as the sample is annealed according to the relation [16].

$$V_{FB} = \varphi_{ms} - \left(\frac{Q'_{ss}}{Cox}\right), \quad (2)$$

Table 2: Electric parameters and conversion efficiencies measured for the Al-BSF cells (#1 to #3) and PERC (#A1 to #A3 and #B1 to #B3).

	Jsc (mA/cm^2)	Voc (mV)	FF (%)	η (%)
Al-BSF #1	37.53	580.09	75.1	16.36
Al-BSF #2	37.19	580.10	76.3	16.46
Al-BSF #3	37.54	570.04	74.8	16.00
PERC #A1	39.43	580.07	74.1	16.95
PERC #A2	38.79	590.05	74.6	17.07
PERC #A3	38.71	590.10	75.0	17.13
PERC #B1	38.90	580.04	73.6	16.62
PERC #B2	38.73	580.08	74.4	16.73
PERC #B3	37.66	590.06	74.1	16.47

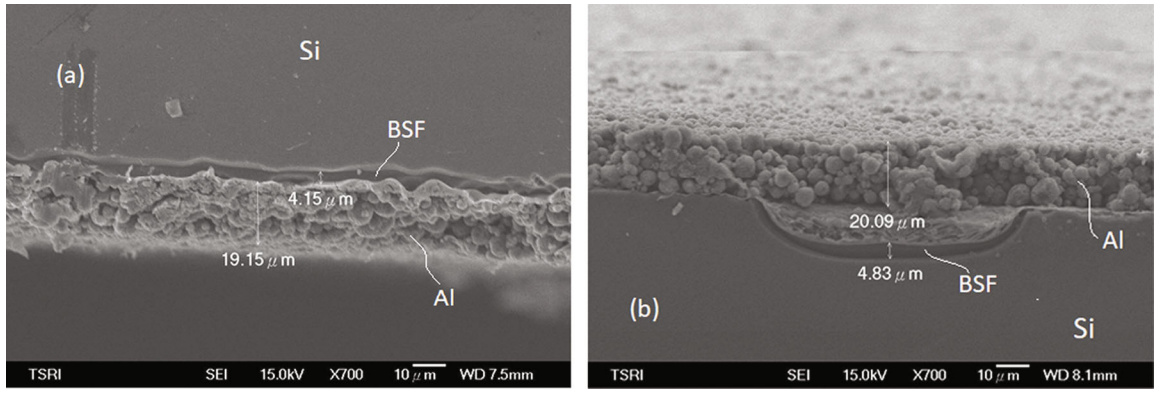

Figure 8: Full BSF for an Al-BSF cell (a) and local BSF for a PERC (b).

where Q'_{ss} is the effective fixed oxide charge, which is negative in the study. And thus, this shifts the CV curve of the annealed sample to the right with respect to the CV curve of the unannealed.

3. Performance of Solar Cells

We have fabricated PERC solar cells with passivation layers formed by the proposed method, with the oxidation and annealing all performed under optimal conditions, i.e., with 10-minute-long oxidation at 400°C, first annealing at 700°C for 3 minutes, and then second annealing at 400°C for 10 minutes. Except for those PERCs, another two groups of cells have also been fabricated. One group is Al-BSF cells, and the other group is PERC fabricated with the first annealing performed under a nonoptimal condition, the latter of which was annealed at 500°C for 6 minutes. Note that a wafer annealed at 500°C for 6 minutes could lead to a lifetime of 10.25 μs in contrast to the lifetime of 45.7 μs for a wafer annealed at the optimal condition.

Table 2 shows the electric and conversion efficiencies measured for these three groups of cells (with 3 cells for each group) under standard test conditions. As seen, Al-BSF cells (see #1 to #3) have lower Jsc and Voc but a higher FF on average compared with the PERC annealed under the optimal condition (see #A1 to #A3). On the other hand, the PERCs annealed under a nonoptimal condition have a higher cell performance than the Al-BSF cells; however, they have a worse performance than the optimal PERC. The optimal PERCs reach an average conversion efficiency of >17%.

The Al-BSF #2 cell and the PERC #A3 cell have a BSF as shown in Figures 8(a) and 8(b), respectively, where the thicknesses of both BSF read >4 μm, respectively. It can be seen from Figure 8(b) that the line trench has a width of ~75 μm. Note that the center-to-center spacing between two adjacent line trenches is 1200 μm in this study, and therefore, the line contact area is ~6.3% of the entire back surface area. Their internal quantum efficiencies (IQEs) as a function of wavelength are shown in Figure 9. The IQE is higher for the PERC relative to the Al-BSF cell at wavelengths smaller than 500 nm and especially at wavelengths longer than 900 nm.

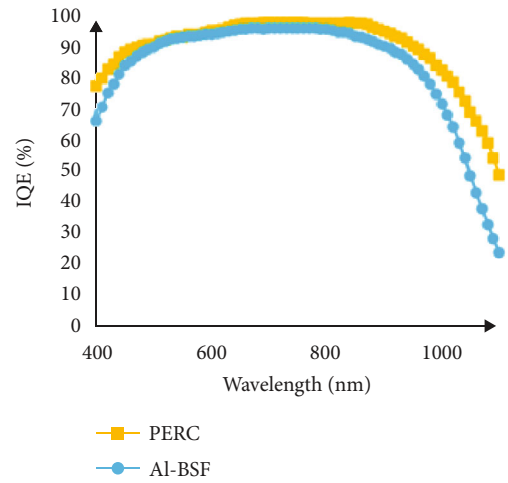

Figure 9: IQE spectra for the cells of PERC#A3 and Al-BSF#2.

We know that the ozone oxidation method applied to form an AlO_x passivation layer can provide a high level of passivation. In the work of Liu et al. [11], they proved that such an oxidation method followed by annealing at 600°C for 90 seconds (without the second annealing) led to a minority carrier lifetime of 41.15 μs and an associated negative charge density of -2.30×10^{12} cm^{-2}. The conversion efficiencies obtained for three PERC were from 16.73% to 16.92%, in contrast to those obtained for two Al-BSF cells, which were around 16.3%. In a subsequent study with the ozone oxidation method, a second annealing process was performed to recover the lifetime back to the level obtained after the first time annealing, which was 40.19 μs. Note that the optimal condition for the first annealing was 700°C and lasted for one minute, and the optimal condition for the second annealing was 400°C and lasted for 20 minutes. Such ozone-treated wafers were then used for the fabrication of three PERCs, with conversion efficiencies ranging from 16.86% to 17.09%, in contrast to the conversion efficiencies of 16.67% to 16.76% obtained for three Al-BSF cells. Obviously, the effect of second annealing on the wafers can be seen in the improvement in conversion efficiency.

4. Conclusion

We have used a thermal oxidation process to oxidize an aluminum thin film into an AlO_x layer on the rear side of a silicon wafer. Through the TEM/EDS/XPS measurements, we confirmed the formation of AlO_x and SiO_x on the rear side and observed an enhanced minority carrier lifetime. The field-effect passivation was further proved in association with the negative charge density at the Si/AlO_x interface. To achieve the maximum lifetime, we found the best oxidation and annealing conditions regarding process temperature and time duration. Under such process conditions, we experimentally confirmed a much lifetime enhancement, which improved the conversion efficiency by a small fraction of one percent. Compared with ozone-treated wafers, the thermally oxidized wafers processed here seem to support a little better passivation owing to a little longer minority carrier lifetime (cp. 45.7 μs for thermal oxidation and 41.15 μs for ozone oxidation). The conversion efficiency of the PERC under study here was thus higher than that of the PERC with an AlO_x passivation layer formed by ozone treatment.

The reported cell performance may not be as good as that of the cell fabricated by applying ALD or PECVD facility for the AlO_x deposition. The reason for this could be manyfold. First, educational laboratories would not have facilities for process lines as sophisticated as those applied by cell manufacturers. Second, wafers for cell fabrication supplied by some merchants are not as good as those used by cell manufacturers. And third, educational labs may use a method that fits into a small-size wafer process, in which machine cutting or laser cutting could damage the cells. However, we have demonstrated that both the previously used ozonation method and the thermal oxidation method used in this study are effective methods for providing good enough passivation, which can be seen from the negative charges produced using either of the two oxidation methods. In this study, a surface charge density of $-3.21 \times 10^{12}\,cm^{-2}$ is reached through the thermal oxidation method, while the ozonation method led to a surface charge density of $-2.63 \times 10^{12}\,cm^{-2}$. More importantly, people will not use toxic chemicals for forming AlO_x passivation layers in the oxidation method.

Data Availability

The raw/processed data for these findings cannot be shared at this time as the data also form part of an ongoing study.

Conflicts of Interest

The authors declare that there is no conflict of interest regarding the publication of this paper.

Authors' Contributions

Ching-Hui Hsu was responsible for the experiment and characterization regarding furnace oxidation. Da-Yao Lao was in charge of providing data for comparison with ozone oxidation with a second annealing technique. Likarn Wang provided substantial contributions to the methodology and manuscript preparation.

Acknowledgments

This research was financially supported by the grant MOST 111-2221-E-007-025 from the National Science and Technology Council, R.O.C.

References

[1] P. Saint-Cast, J. Benick, D. Kania et al., "High-efficiency c-Si solar cells passivated with ALD and PECVD aluminum oxide," *IEEE Electron Device Letters*, vol. 31, no. 7, pp. 695–697, 2010.

[2] R. Kotipalli, R. Delamare, O. Poncelet, X. Tang, L. A. Francis, and D. Flandre, "Passivation effects of atomic-layer-deposited aluminum oxide," *EPJ Photovoltaics*, vol. 4, article 45107, 2013.

[3] C.-H. Hsu, Y.-S. Cho, W.-Y. Wu et al., "Enhanced Si passivation and PERC solar cell efficiency by atomic layer deposited aluminum oxide with two-step post annealing," *Nanoscale Research Letters*, vol. 14, no. 1, 2019.

[4] M. Hofmann, N. Kohn, F. Schwarz et al., "High-power-plasma PECVD of SiNx and Al_2O_3 for industrial solar cell manufacturing," in *Proceedings of 28th European Photovoltaic Solar Energy Conference and Exhibition*, pp. 1184–1187, Paris, France, 2013.

[5] J. A. Töfflinger, A. Laades, C. Leendertz et al., "PECVD-AlO_x/SiN_x passivation stacks on silicon: effective charge dynamics and interface defect state spectroscopy," *Energy Procedia*, vol. 55, pp. 845–854, 2014.

[6] F. Ye, N. Yuan, J. Ding, and Z. Feng, "The performance of thin industrial passivated emitter and rear contacts solar cells with homogeneous emitters," *Journal of Renewable and Sustainable Energy*, vol. 7, no. 1, article 013122, 2015.

[7] T. T. Li and A. Cuevas, "Effective surface passivation of crystalline silicon by rf sputtered aluminum oxide," *Physica Status Solidi (RRL)–Rapid Research Letters*, vol. 3, no. 5, pp. 160–162, 2009.

[8] J. A. García-Valenzuela, R. Rivera, A. B. Morales-Vilches et al., "Main properties of Al_2O_3 thin films deposited by magnetron sputtering of an Al_2O_3 ceramic target at different radio-frequency power and argon pressure and their passivation effect on p-type c-Si wafers," *Thin Solid Films*, vol. 619, pp. 288–296, 2016.

[9] H.-Q. Xiao, C.-L. Zhou, X.-N. Cao et al., "Excellent passivation of p-type Si surface by sol-gel Al_2O_3 films," *Chinese Physics Letters*, vol. 26, no. 8, article 088102, 2009.

[10] Y.-S. Lin, J.-Y. Hung, T.-C. Chen et al., "Effect of post deposition annealing of printed AlO_x film on PERC solar cells," in *2014 IEEE 40th Photovoltaic Specialist Conference (PVSC)*, pp. 0615–0618, Denver, CO, USA, 2014.

[11] P.-K. Liu, Y.-L. Cheng, and L. Wang, "Crystalline silicon PERC solar cell with ozonized AlO_x passivation layer on the rear side," *International Journal of Photoenergy*, vol. 2020, Article ID 6686797, 6 pages, 2020.

[12] C. H. Hsu, *Monocrystalline Silicon PERC Solar Cell With Aluminum Oxide Film Formed by Furnace Oxidation, [M.S. thesis]*, National Tsing Hua University, Hsinchu,

Taiwan, 2020, https://optic2022.conf.tw/site/order/1443/SessionDetail.aspx?lang=en&rmid=H01&sid=1443&snid=H.

[13] K. Kimoto, Y. Matsui, T. Nabatame et al., "Coordination and interface analysis of atomic-layer-deposition Al_2O_3 on Si(001) using energy-loss near-edge structures," *Applied Physics Letters*, vol. 83, no. 21, pp. 4306–4308, 2003.

[14] J. Schmidt, B. Veith, and R. Brendel, "Effective surface passivation of crystalline silicon using ultrathin Al2O3films and Al2O3/SiNxstacks," *Physica Status Solidi (RRL)–Rapid Research Letters*, vol. 3, no. 9, pp. 287–289, 2009.

[15] C.-H. Hsu, C. W. Huang, Y. S. Cho et al., "Efficiency improvement of PERC solar cell using an aluminum oxide passivation layer prepared via spatial atomic layer deposition and post-annealing," *Surface and Coatings Technology*, vol. 358, pp. 968–975, 2019.

[16] D. A. Neamen, *Semiconductor Physics and Devices*, McGraw-Hill, 4th edition, 2012.